JACC: CARDIOONCOLOGY VOL. 3, NO. 1, 2021

ORIGINAL RESEARCH

Cardiac Magnetic Resonance for Early Detection of Radiation Therapy-Induced Cardiotoxicity in a Small Animal Model

El-Sayed H. Ibrahim, PhD,[a,b,c,d] Dhiraj Baruah, MD,[a] Pierre Croisille, MD, PhD,[e] Jadranka Stojanovska, MD,[f] Jason C. Rubenstein, MD,[g] Anne Frei, BS,[h] Rachel A. Schlaak, PhD,[i] Chieh-Yu Lin, MD, PhD,[j] Jamie L. Pipke, BS,[h] Angela Lemke, BS,[k] Zhiqiang Xu, MD, MSc,[l] Amanda Klaas, RVT,[l] Michael Brehler, PhD,[a] Michael J. Flister, PhD,[b,c,k,m] Peter S. Laviolette, PhD,[a,d] Elizabeth M. Gore, MD,[h] Carmen Bergom, MD, PhD[b,c,h,l]

ABSTRACT

BACKGROUND Over one-half of all cancer patients receive radiation therapy (RT). However, radiation exposure to the heart can cause cardiotoxicity. Nevertheless, there is a paucity of data on RT-induced cardiac damage, with limited understanding of safe regional RT doses, early detection, prevention, and management. A common initial feature of cardiotoxicity is asymptomatic dysfunction, which, if left untreated, may progress to heart failure. The current paradigm for cardiotoxicity detection and management relies primarily upon assessment of ejection fraction. However, cardiac injury can occur without a clear change in ejection fraction.

OBJECTIVES We sought to identify cardiac magnetic resonance (CMR) imaging markers of early RT-induced cardiac dysfunction.

METHODS We investigated the effect of RT on global and regional cardiac function and myocardial T1/T2 values at 2 time points post-RT using CMR in a rat model of localized cardiac RT. Rats who received image-guided whole-heart radiation of 24 Gy were compared with sham-treated rats.

RESULTS The rats maintained normal global cardiac function post-RT. However, a deterioration in strain was particularly notable at 10 weeks post-RT, and changes in circumferential strain were larger than changes in radial or longitudinal strain. Compared with sham treatment, circumferential strain changes occurred at the basal, mid-ventricular, and apical levels ($p < 0.05$ for all at both 8 weeks and 10 weeks post-RT), most of the radial strain changes occurred at the mid-ventricular ($p = 0.044$ at 8 weeks post-RT) and basal ($p = 0.018$ at 10 weeks post-RT) levels, and most of the longitudinal strain changes occurred at the apical ($p = 0.002$ at 8 weeks post-RT) and basal ($p = 0.035$ at 10 weeks post-RT) levels. Regionally, lateral myocardial segments showed the greatest worsening in strain measurements, and histological changes supported these findings. Despite worsened myocardial strain post-RT, myocardial tissue displacement measures were maintained, or even increased. T1/T2 measurements showed small nonsignificant changes post-RT compared with values in nonirradiated rats.

CONCLUSIONS Our findings suggest MRI regional myocardial strain is a sensitive imaging biomarker for detecting RT-induced subclinical cardiac dysfunction before compromise of global cardiac function. (J Am Coll Cardiol CardioOnc 2021;3:113–30) © 2021 The Authors. Published by Elsevier on behalf of the American College of Cardiology Foundation. This is an open access article under the CC BY-NC-ND license (http://creativecommons.org/licenses/by-nc-nd/4.0/).

From the [a]Department of Radiology, Medical College of Wisconsin, Milwaukee, Wisconsin, USA; [b]Cardiovascular Center, Medical College of Wisconsin, Milwaukee, Wisconsin, USA; [c]Cancer Center, Medical College of Wisconsin, Milwaukee, Wisconsin, USA; [d]Department of Biomedical Engineering, Medical College of Wisconsin, Milwaukee, Wisconsin, USA; [e]Department of Radiology, Jean-Monnet University, Saint-Etienne, France; [f]Department of Radiology, University of Michigan, Ann Arbor, Michigan, USA; [g]Department of Medicine, Division of Cardiology, Medical College of Wisconsin, Milwaukee, Wisconsin, USA; [h]Department

ISSN 2666-0873 https://doi.org/10.1016/j.jaccao.2020.12.006

ABBREVIATIONS AND ACRONYMS

CMR = cardiac magnetic resonance

ED = end-diastolic

EF = ejection fraction

ESV = end-systolic volume

H&E = hematoxylin and eosin

LAX = long-axis

LV = left ventricle/ventricular

PBST = phosphate buffered saline with Tween

RT = radiation therapy

SAX = short-axis

SS = salt-sensitive

Cancer radiation treatment aims to reduce the risk of recurrence and improve survival by eliminating tumor cells locally that may seed distant metastatic disease. Radiation therapy (RT) is used in more than 50% of all cancer patients, but radiation doses can be limited by side effects to nearby organs, especially the heart for patients with thoracic tumors. Radiation-induced cardiac dysfunction can occur months to years following cardiac RT exposure, and cardiac sequelae can include a number of clinical manifestations, including ischemic heart disease, fibrosis, arrhythmias, cardiomyopathy, valvular abnormalities, and/or pericarditis (1,2). RT plays an integral role in treating breast cancer, as well as advanced lung cancer (3–6), and studies in lung cancer patients have found that mortality correlates with mean heart dose (3), or with the percent of the heart receiving 5 Gy (7), 30 Gy, and/or 50 Gy (5). However, it is unclear what radiation doses to the heart pose the most risk in lung cancer patients (8), which is likely due to inherent challenges in addressing the case-by-case variability of incidental cardiac radiation in these patients. Preclinical models using defined radiation dose distributions and sensitive imaging to assess regional cardiac function are ideal to meet many of these identified challenges for radiation oncologists treating thoracic tumors (9). Identification of an imaging protocol that can allow for sensitive, regional detection of subclinical radiation-induced cardiac dysfunction in preclinical models would advance knowledge of how radiation affects cardiac function, and ultimately lead to better dose guidelines for radiation therapy and decrease the incidence and severity of radiation-induced cardiotoxicity.

The most common initial feature of cardiotoxicity is asymptomatic systolic left ventricular (LV) dysfunction, which if left untreated may progress to congestive heart failure (10,11). This initial cardiac dysfunction may not be clinically apparent for many years because of cardiac function normalization by compensatory mechanisms. The current paradigm for cardiotoxicity detection and management relies primarily upon the assessment of LV ejection fraction (EF). Although EF is important, it may not reflect the underlying advancement of subclinical cardiovascular disease that could portend the development of treatment-induced cardiovascular events (12).

Cardiac magnetic resonance (CMR) imaging is considered the reference standard for the evaluation of cardiac volumes, mass, and function. Further, parameters that reflect global and regional function, such as myocardial strain, are more sensitive than EF for early recognition of asymptomatic cardiac dysfunction and identification of patients at risk of heart failure (13,14). Although changes in these parameters have been widely studied following cancer treatment in specific cancer populations such as breast cancer (15), the clinical value of these imaging biomarkers has not been comprehensively defined with RT treatment or in lung cancer patients. In this study, we investigated CMR capabilities for regional cardiac function analysis and tissue characterization for evaluation of cardiac performance and early detection of RT-induced cardiotoxicity in a lung cancer rat model of image-guided localized cardiac RT (16). We evaluated early time points before the compromise of global function but when inflammatory changes could be observed (9,16), and we compared the results to sham-treated control rats.

METHODS

ANIMAL MODEL OF RT. This study was approved by our institutional animal care committee. Inbred salt-sensitive (SS) rats were housed in pathogen-free conditions with a 12:12-h light:dark cycle and administered a standard diet (0.4% salt) (9). A total of 22 SS adult female rats, 10 to 12 weeks of age, were randomized (1:2) into 2 groups: sham-treated (n = 7) and cardiac RT (n = 15). The RT group received image-guided localized whole-heart radiation of 24 Gy in 1 fraction (3 equally weighted beams: 1 anterior-posterior beam and 2 lateral beams, 1:1:1, 225 kVp, 13

of Radiation Oncology, Medical College of Wisconsin, Milwaukee, Wisconsin, USA; [i]Department of Pharmacology and Toxicology, Medical College of Wisconsin, Milwaukee, Wisconsin, USA; [j]Department of Pathology & Immunology, Washington University School of Medicine, St. Louis, Missouri, USA; [k]Department of Physiology, Medical College of Wisconsin, Milwaukee, Wisconsin, USA; [l]Department of Radiation Oncology, Washington University School of Medicine, St. Louis, Missouri, USA; and the [m]Genomic Sciences and Precision Medicine Center, Medical College of Wisconsin, Milwaukee, Wisconsin, USA.

The authors attest they are in compliance with human studies committees and animal welfare regulations of the authors' institutions and Food and Drug Administration guidelines, including patient consent where appropriate. For more information, visit the Author Center.

Manuscript received April 1, 2020; revised manuscript received December 3, 2020, accepted December 7, 2020.

mA, 0.32-mm Cu, 2.69 Gy/min), as previously described (16).

CMR SCANS. Rats were imaged on a small-animal 9.4-T MRI scanner (Bruker, Ettlingen, Germany) using a 4-element surface coil at 8 and 10 weeks post-RT or 8 weeks post-sham treatment. The implemented CMR scan included acquiring both long-axis (LAX) and short-axis (SAX) cine and tagged images, as previously described (17). In addition, inversion recovery T1 mapping and multiecho spin-echo T2 mapping techniques were used to acquire relaxometry maps in mid-ventricular SAX slices (17). Total scan time was approximately 1 h.

CMR IMAGE ANALYSIS AND STATISTICS. The cine, inversion recovery, and multiecho spin-echo images were analyzed using the cvi42 software version 5.11 (Circle Cardiovascular Imaging, Calgary, Canada) to measure ventricular EF, mass, end-diastolic (ED) volume, end-systolic volume (ESV), stroke volume, and T1/T2 maps. The tagged images were analyzed using the SinMod technique (InTag, Lyon, France) (18) to measure myocardial circumferential, radial, and longitudinal strain, as well as tissue rotation angle, SAX motion, and LAX motion, where the reproducibility of the CMR measures have been previously demonstrated (18). Analysis was performed in a blinded fashion to avoid bias. Regional cardiac function parameters were measured at different myocardial segments, and results were represented using the American Heart Association 17-segment model.

TISSUE ARCHITECTURE AND MEASUREMENT OF CARDIAC FIBROSIS, MAST CELLS, AND VASCULARIZATION. Ten weeks after RT or sham treatment, rats were euthanized by isoflurane overdose, hearts were excised and rapidly rinsed with phosphate buffered saline, and a SAX mid-ventricular section was excised for histology. The heart sections were fixed in zinc formalin for 48 h, transferred to 70% ethanol, and then embedded in paraffin. Four-micrometer sections were stained with hematoxylin and eosin (H&E) using standard methods. H&E slides from the hearts were examined for architectural changes, such as hemorrhage, cellular vacuolization, and/or cellular necrosis in the interventricular septum or left ventricular lateral wall (n = 4 to 5/condition). These changes were scored blindly by a board-certified pathologist (C.L.).

For immunofluorescent staining of blood vessels and cardiomyocytes, all antibodies were diluted 1:100 in phosphate buffered saline with Tween (PBST, pH 7.4, 0.1% Tween-20) containing 5 mg/ml of bovine serum albumin. Frozen sections were fixed with formalin for 1 min, rehydrated in PBST for 10 min, and incubated for 1 h at 37°C with primary antibodies against the blood vessel marker, Sh2b3 (HPA005483, Sigma-Aldrich, St. Louis, Missouri) (19) and cardiomyocyte marker Caveolin-3 (610420, BD Biosciences, San Jose, California) (20). Slides were then washed with PBST for 10 min and incubated for 1 h at 37°C with secondary antibodies conjugated with Alexa Flour 488 or Alexa Fluor 555 (Jackson ImmunoResearch, West Grove, Pennsylvania), followed by an additional 10-min wash in PBST. Slides were mounted in Vectashield medium containing 4,69-diamidino-2-phenylindole nuclear stain (Vector Laboratories, Burlingame, California). Images were obtained from the LV lateral wall where cross-sectioned cardiomyocytes and capillaries were visualized. All images were acquired using a Nikon Eclipse 55i upright microscope equipped with a Nikon SD-2MBW camera and NIS Elements D software version 5.02.01 (Nikon Instruments, Melville, New York). Staining was quantified on blinded samples by counting the number of capillaries abutting each cardiomyocyte in 3 to 4 high-powered fields per heart (n = 3), as previously described (21–24).

For fibrosis quantification, Masson's trichrome staining for collagen deposition was performed on fixed 4-μm sections. Images were acquired using Nikon Eclipse 50i upright microscope and Digital DS-U3 camera. ImageJ software version 1.38 (NIH, Bethesda, Maryland) was used to quantify interstitial collagen, taking blue area/(total area − white space). In a blinded manner, 4 to 5 hearts/condition were analyzed, with 5 fields per samples quantified in areas lacking visualized blood vessels so as to exclude the contribution of perivascular fibrosis. Perivascular fibrosis in coronary vessels (<50 μm) was quantified separately using ImageJ software, and expressed as % fibrosis per lumen area, with at least 5 vessels quantified per field, with 3 to 4 hearts examined per condition, and 15 to 20 vessels per condition analyzed. Mast cell staining was performed using toluidine blue as previously described (16). Four high-powered fields were quantified per sample, with n = 4 animals examined per condition. Cells were quantified in the myocardium by 2 independent investigators (Z.X. and A.K.) blinded to the sample treatments.

STATISTICAL ANALYSIS. SPSS Statistics version 24 (IBM, Armonk, New York) and Excel Microsoft Office 365 version (Microsoft, Redmond, Washington) were used for statistical analysis. Measurements are represented as mean ± SEM. The Student's *t*-test was used to determine significant measurement changes between CMR measurements according to different groups and for the analysis of immunofluorescent and

FIGURE 1 Mast Cell Infiltration in the Myocardium After Localized Cardiac RT

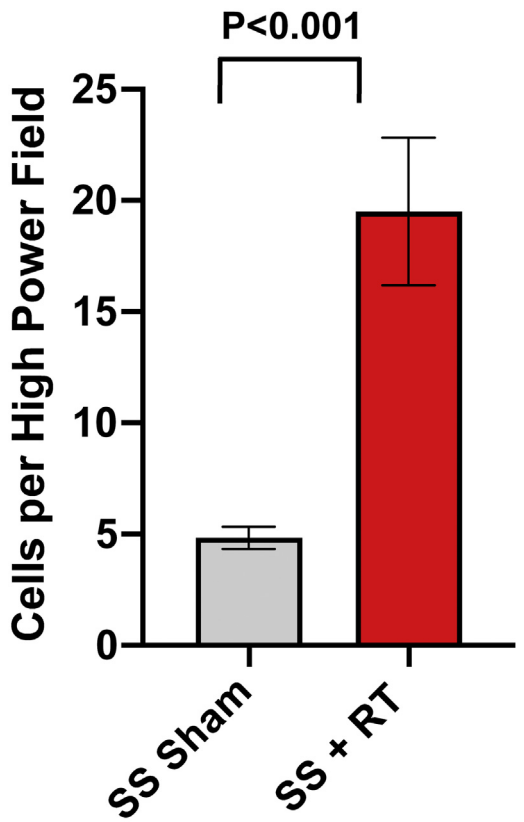

Adult female rats were administered 24 Gy of localized cardiac radiation therapy (RT) or sham treatment, and at 10 weeks post-treatment, their hearts were harvested. Mast cells were stained using toluidine blue and quantified. The figure shows a significant increase in mast cell infiltration after RT, n = 4/condition. Values are mean ± SEM. SS = salt-sensitive.

immunohistochemical data ($p < 0.05$ considered significant). Post-hoc Bonferroni correction was used to adjust p values for multiple comparisons.

RESULTS

HISTOPATHOLOGIC CHANGES IN THE RAT HEART OCCUR BY 10 WEEKS AFTER LOCALIZED CARDIAC RT. SS rats developed cardiac dysfunction, as measured via echocardiogram at 12 to 20 weeks after 24 Gy of cardiac RT (16). However, no significant decrease in EF was seen at 12 weeks post-RT in this model. For this study, we specifically focused on earlier time points, during periods where inflammatory changes occur (9,16) that may be detectable via CMR. At 10 weeks post-RT, there was a significant increase in mast cells in the myocardium after RT, compared with sham treatment (Figure 1). We also examined myocardial damage and microvascular density in SS hearts 10 weeks post-RT. H&E-stained sections from sham-treated hearts demonstrated no cellular vacuolization or necrosis in the myocardium (Figures 2A and 2B), whereas myocardial damage was seen in the RT-treated hearts (Figures 2C and 2D). Hemorrhage was also seen in the radiated hearts (Figures 2C and 2D). In general, there was more notable necrosis and vacuolization in the LV lateral wall (Figure 2D) than the interventricular septum (Figure 2C). Vascularity was quantified using the number of vessels/cardiomyocyte (21), which demonstrated a marginally significant decrease of microvascular density in irradiated rat hearts post-RT, as compared with nonirradiated, sham-treated animals at 10 weeks after treatment (Figures 2E and 2F), although the difference was not statistically significant (sham vs. RT 3.25 ± 0.68 vs. 1.65 ± 0.32; $p = 0.101$) (Figure 2G). In addition, there was an increase in interstitial fibrosis at 10 weeks post-RT compared with sham, although this was also not statistically significant (0.41 ± 0.16 vs. 0.79 ± 0.14; $p = 0.080$) (Figures 3A to 3C). Similarly, there was a small, but nonsignificant, increase in perivascular fibrosis in the LV (Figures 3D to 3F).

CARDIAC FUNCTION IS MAINTAINED UP TO 10 WEEKS POST-HIGH-DOSE WHOLE-HEART RT. We conducted CMRs at 8 and 10 weeks after 24 Gy of localized cardiac radiation, when inflammatory changes were significantly different between sham-treated and RT-treated animals, but fibrosis and vascular density showed more modest differences between the rats receiving RT compared with nonirradiated sham controls. At these time points, local radiation changes, such as hair loss at the RT-beam entry sites, were occurring, but systemic changes such as weight loss were absent (data not shown). Figure 4 and Videos 1 to 4 show representative ED and end-systolic cine images of RT and control rats at 8 weeks post-treatment. These revealed preserved cardiac function with cardiac remodeling and hypertrophy after RT. Global cardiac function was normal in all rats (Table 1), with increased EF and myocardial mass, and decreased ESV and end-diastolic volume in the RT compared with nonirradiated rats.

MYOCARDIAL STRAIN IS A SENSITIVE MARKER OF EARLY RT-INDUCED CARDIOTOXICITY. Segmental strain curves during the whole cardiac cycle in sham-treated, 8 weeks post-RT, and 10-week post-RT rats are shown in Figure 5. Despite normal global function, strain measurements showed reduced strain in the RT rats compared with nonirradiated controls.

FIGURE 2 SS Rats and Myocardial Vacuolization and Necrosis

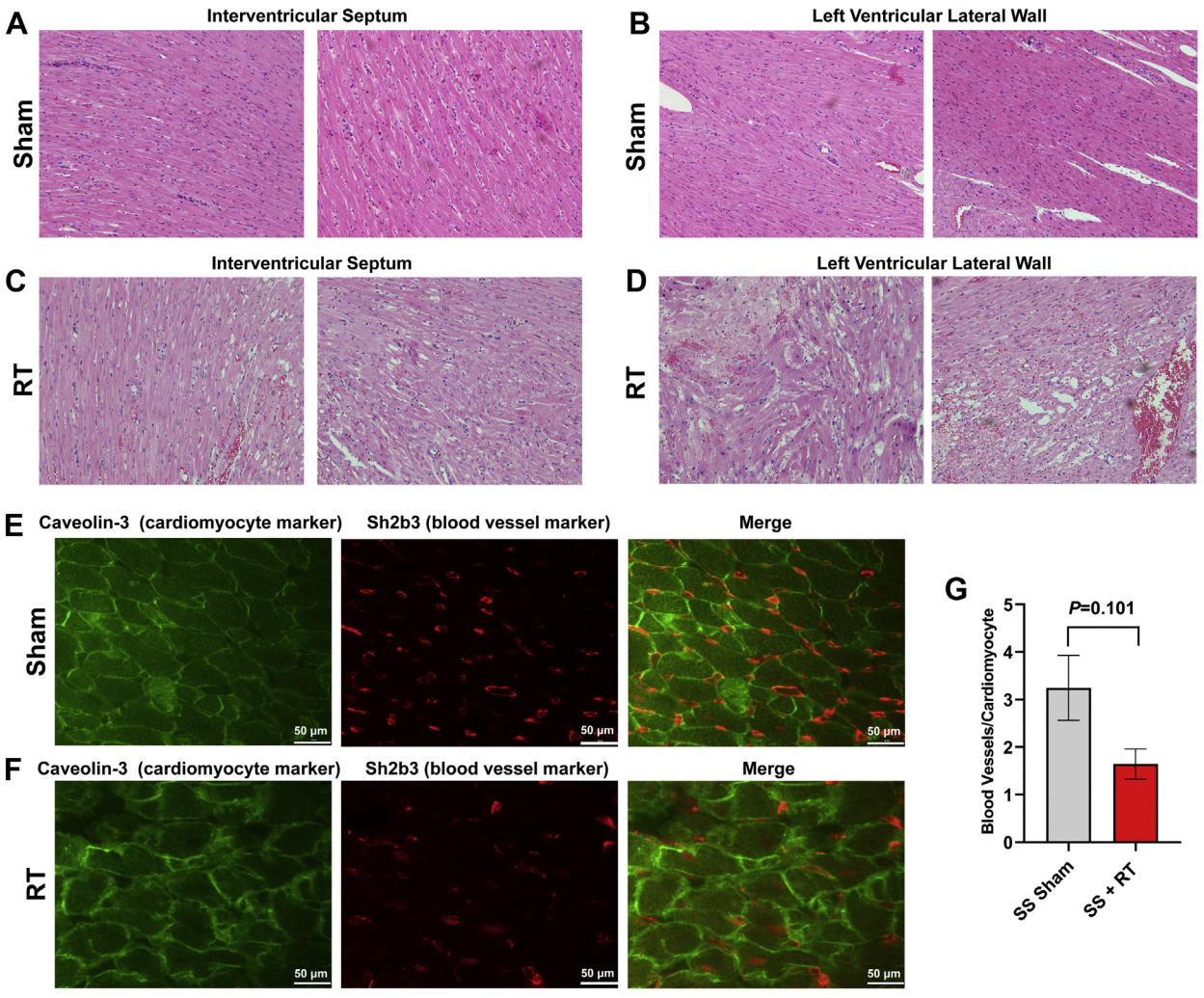

SS rats demonstrate myocardial vacuolization and necrosis, with a marginally significant decrease of microvascular density, 10 weeks after 24-Gy localized cardiac RT. Adult female rats were administered 24 Gy of localized cardiac RT or sham treatment, and at 10 weeks post-treatment, their hearts were harvested. Hematoxylin and eosin–stained sections demonstrated healthy left ventricular (LV) myocardial tissue in sham-treated hearts **(A and B)**, whereas RT-treated hearts had notable necrosis and vacuolization **(C and D)**, which was increased in the LV lateral wall **(D)** when compared with the interventricular septum **(C)**. **(E to G)** Fixed heart sections were stained for cardiomyocytes (caveolin-3) and blood vessels (Sh2b3). The number of blood vessels per cardiomyocyte was calculated, with representative images from sham-treated **(E)** and RT-treated **(F)** hearts. This demonstrated a marginally significant decrease of capillary density after RT **(G)**. n = 3/condition. Values are mean ± SEM. Abbreviations as in Figure 1.

Furthermore, the curves show lack of synchrony for contraction of different segments at 10 weeks post-RT. Values for global, basal, mid-ventricular, and apical myocardial strain are shown in Table 2, Figure 6, and the Central Illustration, which demonstrate reduced strain post-RT with altered patterns between different myocardial segments.

TISSUE CONTRACTILITY PATTERNS POST-RT ARE AFFECTED BY LOCATION OF DIFFERENT MYOCARDIAL SEGMENTS. On a regional basis, different myocardial segments showed different temporal patterns of change in strain post-RT, as shown in Figure 7 and Table 2. For circumferential strain, most strain reductions between the sham-treated and 8-week post-RT rats occurred at the basal (anterior and anterolateral segments), mid-ventricular (all but the inferior segments), and apical (all but the lateral segments) levels (Figure 7A). The greatest reduction in circumferential strain at 10 weeks post-RT, compared with 8 weeks post-RT, occurred at the basal (all but the

FIGURE 3 SS Rats and Increase in Fibrosis

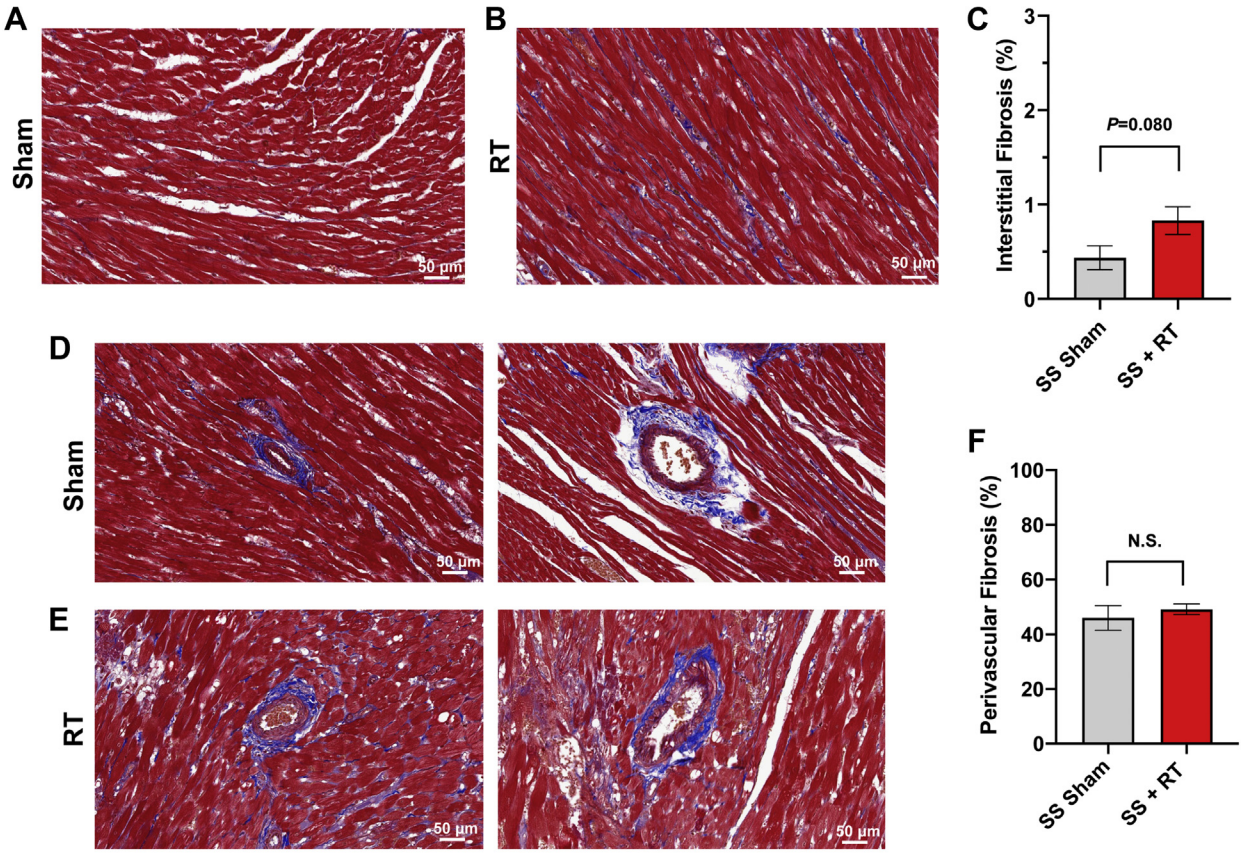

SS rats demonstrate no appreciable increase in fibrosis 10 weeks after 24-Gy localized cardiac RT. Ten weeks after 24 Gy of localized cardiac RT or sham treatment, Masson's trichrome staining was performed, and the interstitial and perivascular fibrosis was quantified. There was a nonsignificant increase in interstitial **(A to C)** and perivascular **(D to F)** fibrosis in the RT-treated hearts. n = 4 to 5/condition. Values are mean ± SEM; p = 0.476. Abbreviations as in Figure 1.

anterior segments) and mid-ventricular (anterolateral and inferolateral segments) levels. Although circumferential strain worsened between the 8 weeks post-RT and 10 weeks post-RT at the basal and mid-ventricular levels, it was mostly maintained at the apical level between these 2 time points.

For radial strain, most reductions between the nonirradiated and 8-week post-RT rats occurred at the basal (inferior and inferolateral), mid-ventricular (anterior, anterolateral, and inferior), and apical (septal only) levels (Figure 7B). Compared with sham, although radial strain decreased at the basal and mid-ventricular levels, it increased at the apical level. Most of the reductions in radial strain at 10 weeks post-RT, compared with 8 weeks post-RT, occurred at the basal (anterior and inferior), mid-ventricular (inferolateral only), and apical (anterior only) levels. Although radial strain decreased at the basal level, it was mostly maintained at the mid-ventricular and apical levels between 8 and 10 weeks.

For longitudinal strain, changes between the nonirradiated control and 8-week post-RT rats were qualitatively greater than the changes between 8 and 10 weeks post-RT (Figure 7C). Most of the reductions between the nonirradiated and 8-week post-RT rats occurred at the apical level, whereas most of the worsening between 8- and 10-week post-RT longitudinal strain occurred in the basal lateral regions (Figure 7C). Apical longitudinal strain at 10 weeks post-RT was worse than that in the nonirradiated rats, but improved compared with rats 8 weeks post-RT.

TISSUE DISPLACEMENT IS MAINTAINED UP TO 10 WEEKS AFTER WHOLE-HEART HIGH-DOSE RT. Tissue displacement analyses are shown in Figure 8 and Table 3. The rotation angle decreased at the basal level and increased at mid-ventricular and apical

FIGURE 4 **Cine Images of RT and Sham-Treated Rats**

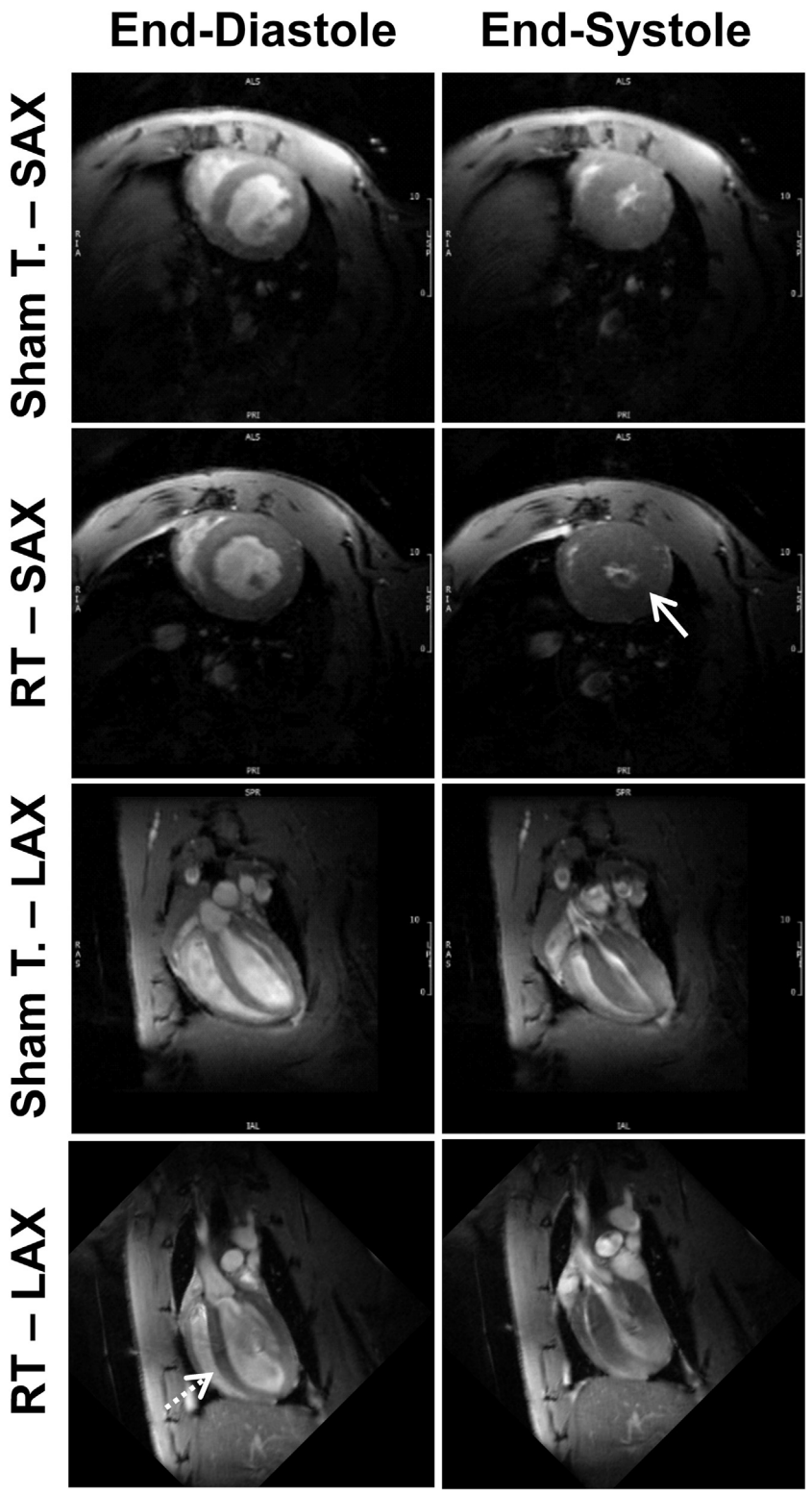

Cine images of radiation therapy (RT) and sham-treated (Sham T.) rats demonstrate ventricular remodeling and hypertrophy post-RT. Short-axis (SAX) and long-axis (LAX) cine cardiac magnetic resonance images showing end-diastolic (ED) and end-systolic (ES) slices in both sham-treated and RT-treated rats at 8 weeks post-treatment. The images show preserved global cardiac function post-RT, along with hypertrophy **(solid arrow)** and cardiac remodeling **(dotted arrow)** compared with sham-treated rats.

TABLE 1 Global Cardiac Function Parameters at Different Time Points Post-RT

	8 Weeks			10 Weeks	
	Sham-Treated Controls	Post-RT	p Value vs. Control	Post-RT	p Value vs. Control
LV EF, %	67.0 ± 2.6	78.0 ± 0.7	0.003	79.0 ± 0.9	0.002
LV mass, g	0.38 ± 0.01	0.49 ± 0.02	<0.001	0.56 ± 0.01	<0.001
LV EDV, ml	0.29 ± 0.01	0.259 ± 0.010	0.022	0.263 ± 0.010	0.014
LV ESV, ml	0.10 ± 0.007	0.060 ± 0.004	<0.001	0.060 ± 0.003	<0.001
LV SV, ml	0.190 ± 0.008	0.200 ± 0.007	0.317	0.200± 0.005	0.141
RV EF, %	69.0 ± 1.2	73.0 ± 1.6	0.039	72.0 ± 1.6	0.038
RV mass, g	0.070 ± 0.002	0.100 ± 0.009	0.009	0.130 ± 0.008	<0.001
RV EDV, ml	0.140 ± 0.005	0.120 ± 0.008	0.113	0.130 ± 0.009	0.300
RV ESV, ml	0.040 ± 0.003	0.030 ± 0.002	0.007	0.030 ± 0.004	0.047
RV SV, ml	0.100 ± 0.005	0.090 ± 0.007	0.639	0.100 ± 0.006	0.556

Values are mean ± SEM.
EDV = end-diastolic volume; EF = ejection fraction; ESV = end-systolic volume; LV = left ventricular; RT = radiation therapy; RV = right ventricular; SV = stroke volume.

levels between the sham-treated and 8-week post-RT rats, whereas it was maintained at all levels between 8 and 10 weeks post-RT (Figure 8). Most of the reductions in rotation angle occurred between the nonirradiated control and 8-week post-RT rats at the basal inferior and inferolateral segments. Most of the increases in rotation angle between the nonirradiated and 8-week post-RT rats occurred at the basal (anterolateral segments), mid-ventricular (anterior, anterolateral, and inferolateral segments), and apical (septal segment) levels, whereas most of the increases in rotation angle between 8 and 10 weeks post-RT occurred at the basal (inferior segments), and mid-ventricular and apical (anterior segments) levels (Figure 8).

Changes in tissue motion showed different patterns in the SAX and LAX directions, as shown in Table 3. Changes in SAX motion between the nonirradiated control and 8-week post-RT rats were larger than measurement changes between 8 and 10 weeks post-RT. Similar to the rotation angle's temporal change pattern, SAX motion decreased at the basal level and increased at the mid-ventricular and apical levels between the sham-treated and 8-week post-RT rats, whereas it decreased, increased, and was maintained at the basal, mid-ventricular, and apical levels, respectively, between 8 and 10 weeks post-RT (Figure 8). On the other hand, global LAX motion showed a notable increase post-RT, as shown in Table 3. LAX motion decreased at the basal level and increased at mid-ventricular and apical levels between the sham-treated and 8-week post-RT rats, whereas it increased at all levels between the 8- and 10-week post-RT rats.

MYOCARDIAL T1/T2 VALUES SHOW SMALL CHANGES AFTER HIGH-DOSE CARDIAC RT. Figure 9 shows representative T1 and T2 maps. Apparent myocardium T1 values were 647 ± 26 ms, 619 ± 17 ms (p = 0.405), and 655 ± 15 ms (p = 0.796) in the sham-treated, 8-week, and 10-week post-RT rats, respectively. In general, T1 values were not significantly different between different rat groups, although T1 values at 10 weeks post-RT were closer to those in sham-treated rats than to the values at 8 weeks post-RT. Average myocardium T2 values were 12.7 ± 0.3 ms, 16.2 ± 0.4 ms (p = 0.001), and 14.7 ± 0.6 ms (p = 0.041) in the sham-treated, 8-week, and 10-week post-RT rats, respectively, where the T2 values post-RT were elevated, especially at 8 weeks post-RT, compared with T2 values in the sham-treated rats. The differences in the T2 values between 8 weeks and 10 weeks post-RT were not statistically significant.

DISCUSSION

In this study, we investigated the effect of RT on global and regional cardiac function and myocardial T1/T2 values using CMR in a rat model of high-dose localized whole-heart irradiation, and we also examined potential histological correlates of CMR changes seen after cardiac RT. Histological analysis of the irradiated cardiac tissue correlates with increased changes seen in the LV lateral wall when compared with the septum, with increased vacuolization and necrosis seen in the lateral wall. In addition, changes in edema manifesting on CMR may be due to inflammation, as increased mast cell infiltration (Figure 1) (16) and T-cell infiltration (25) is seen after cardiac RT. To the best of our knowledge, this is the first study to investigate RT-induced cardiotoxicity effects on regional cardiac function and histological changes associated with this dysfunction in such detail.

In this model, we utilized a single high dose of RT localized to the heart of SS female rats to provide

FIGURE 5 Strain Curves in Sham-Treated and RT Rats

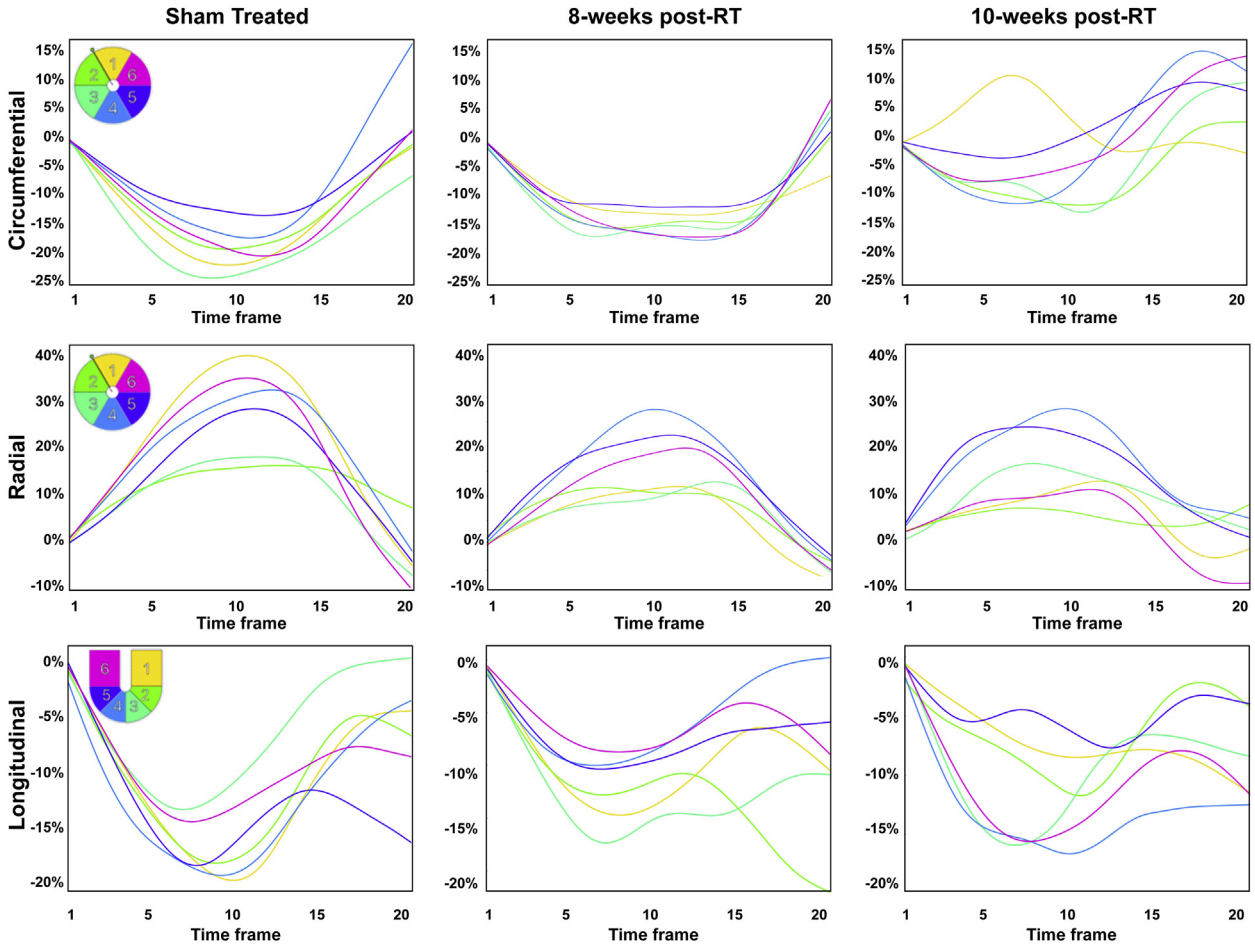

Strain curves in sham-treated and radiation therapy (RT) rats demonstrate reduced strain and altered patterns post-RT. Representative circumferential, radial, and longitudinal strain curves across different myocardial segments in the left ventricle throughout the cardiac cycle in sham-treated, 8-week, and 10-week post-RT rats. Color code is shown in the **upper left corner of the left panels** for mid-ventricular short-axis segments (1, anterior; 2, anteroseptal; 3, inferoseptal; 4, inferior; 5, inferolateral; 6, anterolateral) and 4-chamber long-axis segments (1, basal-lateral; 2, mid-lateral; 3, apical-lateral; 4, apical-septal; 5, mid-septal; 6, basal-septal). The strain curves show strain values throughout the whole cardiac cycle (20 heart phases), starting with time frame #1 immediately after the electrocardiogram R-wave, through end-systole at time frame #9 or #10 until end-diastole at time frame #20. Overall, peak strain worsens post-RT. Furthermore, the curves show lack of synchrony for contraction of different segments at 10 weeks post-RT.

proof-of-principle that CMR can identify RT-induced cardiac changes. This model of RT has previously been published (9,16), and the 24-Gy single dose of RT has been shown to result in long-term cardiac damage similar to the multifraction regimen of 9 Gy ×5 (16,25). Due to the need for daily anesthesia for image-guided RT in our models, as well as the time required for these daily treatments, regimens that mirror clinical treatments lasting many weeks are not feasible in our small animal model. Although the exact doses and fractionations used in our models are not received clinically to the whole heart, high doses of fractionated RT to regions of the heart do occur in subsets of patients receiving high doses of RT or RT with concurrent or sequential chemotherapy (5,26). In other situations, such as some malignancies more common in children and young adults, the whole heart still receives radiation exposure as part of their cancer treatment radiation prescription (27). In the current study, using high-dose cardiac RT to the

TABLE 2 Myocardial Strain Measurements in RT and Control (Sham-Treated) Rats

	8 Weeks			10 Weeks	
	Sham-Treated Control	Post-RT	p Value vs. Control	Post-RT	p Value vs. Control
Circumferential					
Global	−14.1 ± 0.8	−10.2 ± 0.3	0.002	−8.4 ± 0.2	<0.001
Base	−14.0 ± 0.9	−11.2 ± 0.6	0.017	−8.4 ± 0.5	<0.001
Mid	−15.0 ± 0.7	−10.8 ± 0.3	<0.001	−9.1 ± 0.5	<0.001
Apex	−12.3 ± 1.2	−7.8 ± 1.0	0.012	−8.0 ± 0.9	0.011
Radial					
Global	23.3 ± 1.5	21.7 ± 1.5	0.270	20.9 ± 2.0	0.201
Base	23.7 ± 2.3	19.8 ± 0.8	0.076	16.9 ± 1.8	0.018
Mid	26.6 ± 1.8	22.3 ± 1.4	0.044	22.7 ± 2.3	0.107
Apex	18.6 ± 2.7	23.7 ± 4.5	0.201	24.2 ± 4.0	0.143
Longitudinal					
Global	−15.6 ± 0.7	−12.3 ± 0.4	0.002	−12.7 ± 0.6	0.004
Base	−14.9 ± 1.3	−13.6 ± 2.0	0.271	−12 ± 1.7	0.035
Mid	−16.9 ± 0.5	−14.3 ± 1.3	0.094	−14 ± 1.0	0.059
Apex	−14.9 ± 0.6	−9.0 ± 1.3	0.002	−12 ± 0.2	0.093

Values are mean ± SEM.
RT = radiation therapy,

whole heart, we observed an increase in LV EF at 8 to 10 weeks post-RT (**Figure 4**). This is consistent with previously published results at 12 weeks post-RT, where LV EF is preserved initially and subsequently decreases by 20 weeks post-RT (16). The increase in EF post-RT was accompanied by significant cardiac hypertrophy. RV EF also increased post-RT, but this was not statistically significant. Similarly, although both LV and RV ESV decreased post-RT compared with nonirradiated rats, this decrease was significant only for the LV, and not for the RV. In this study, both LV and RV myocardial mass increased post-RT (**Table 1**). We hypothesize that this reflects cardiac remodeling to maintain global function and/or inflammation in the face of acute injury from RT. Previous work has demonstrated that cardiac hypertrophy in this model is dependent upon adaptive immunity, animal sex, and/or strain (16,25).

Despite normal EF, worsening in myocardial strain revealed subclinical cardiac dysfunction, where different strain components helped characterize the nature of these abnormal patterns (**Central Illustration**). Interestingly, apical circumferential strain, and both mid-ventricular and apical radial strain were maintained between 8 and 10 weeks post-RT, and apical radial strain increased at 8 weeks post-RT compared with sham-treated rats. The changes in circumferential strain post-RT were more substantial than the changes in radial or longitudinal strain. Compared with sham treatment, changes in circumferential strain occurred at the basal, mid-ventricular, and apical levels; most of the changes in radial strain occurred at the mid-ventricular level; and most changes in longitudinal strain occurred at the apical level, with less substantial changes at the basal segments for all strain dimensions. Lateral myocardial segments showed significant changes in strain measurements at 10 weeks post-RT (**Figure 7**), which may be related to increased myocardial tissue vacuolization and necrosis in the lateral wall versus the interventricular septum in our animal model (**Figures 2C and 2D**). Although myocardial strain values worsened post-RT, the tissue displacement parameters showed nonsignificant increases post-RT, especially at mid-ventricular and apical levels, with LAX motion showing more increase post-RT versus SAX motion or rotation angle. This paradoxical increase in tissue motion post-RT may be due to ongoing remodeling to maintain global cardiac function despite the observed deterioration in different strain dimensions.

Although rats were prescribed 24 Gy to isocenter using 3 equally weighted beams, due to differences in tissue density, anatomy, and other factors, the whole heart does not receive a uniform dose of 24 Gy (16). Unfortunately, detailed dosimetric data for the 17 LV segments was not possible to obtain due to limitations with the computed tomography-guided irradiator-obtained noncontrast computed tomography imaging and planning software limitations. However, crude dosimetric analysis of a representative female rat treated with 24 Gy of localized RT indicates that due to anatomy and beam arrangements, the inferior basal and inferior apical areas may receive higher doses than other surrounding areas (data not shown). Additional studies with improved methodologies will help to further define whether different segments of the heart are more sensitive to a given dose of irradiation.

The myocardial T1 and T2 values showed different patterns post-RT compared with sham treatment. The changes in T1 values were nonsignificant; therefore, these changes could be due to measurement variability and limited sample size. The T2 values slightly increased at 8 weeks post-RT and then decreased at 10 weeks post-RT. T1 and T2 values have been used for the assessment of changes in tissue composition, for example, fibrosis or generic myocardial tissue damage (T1 increase) and edema (T2 increase) (28), which may be part of the subacute and/or late cardiac

FIGURE 6 Strain Measurements in RT and Sham-Treated Rats

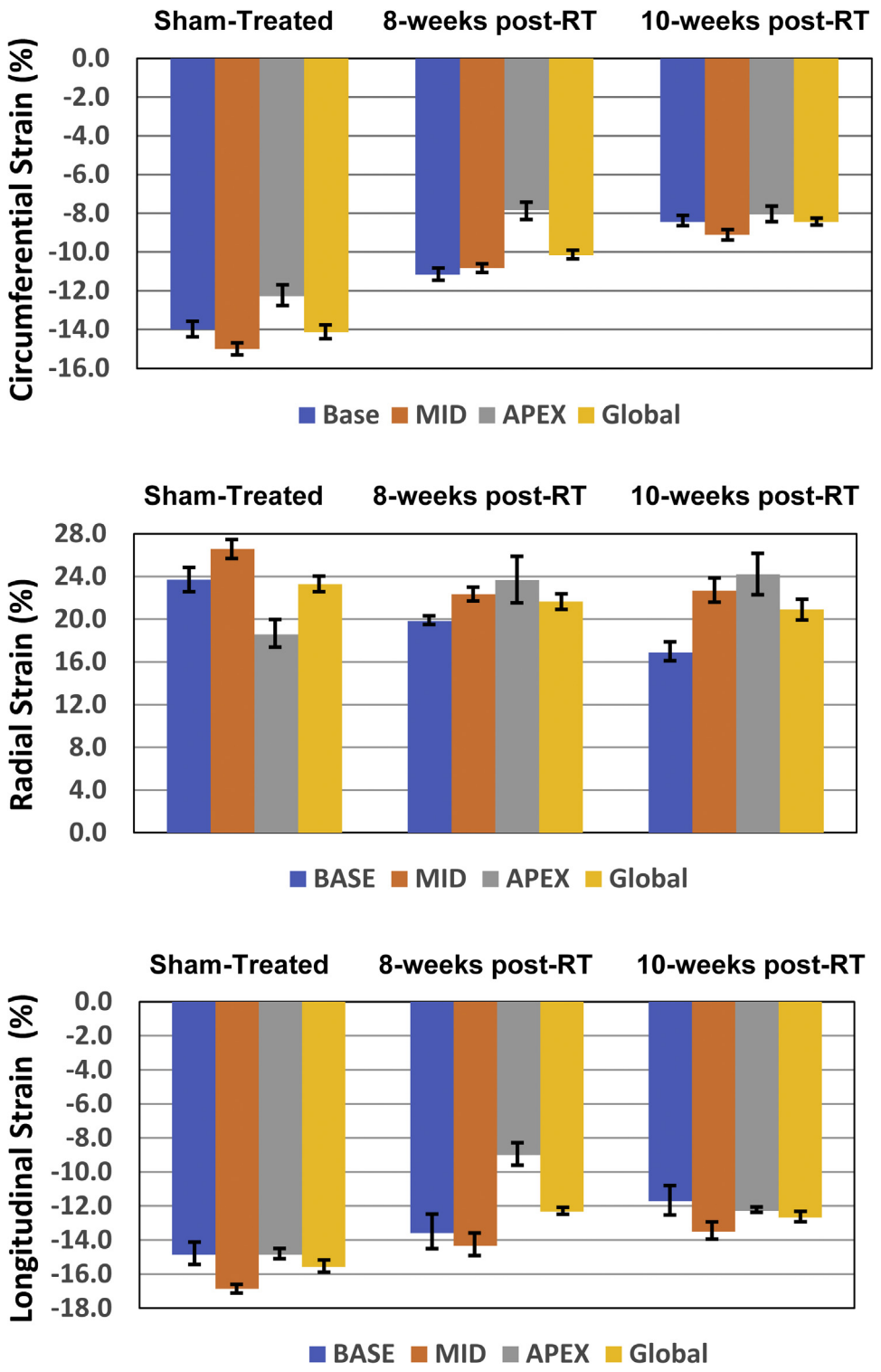

Strain measurements in radiation therapy (RT) and sham-treated rats reveal early worsening in strain, especially in the circumferential direction, post-RT. Compared with sham, circumferential strain changes occurred at the basal, mid-ventricular, and apical levels ($p < 0.05$ for all), especially at the lateral regions, which suggests that circumferential strain is a sensitive marker of RT-induced cardiotoxicity.

FIGURE 7 Segmental Strain Distribution in RT and Sham-Treated Rats

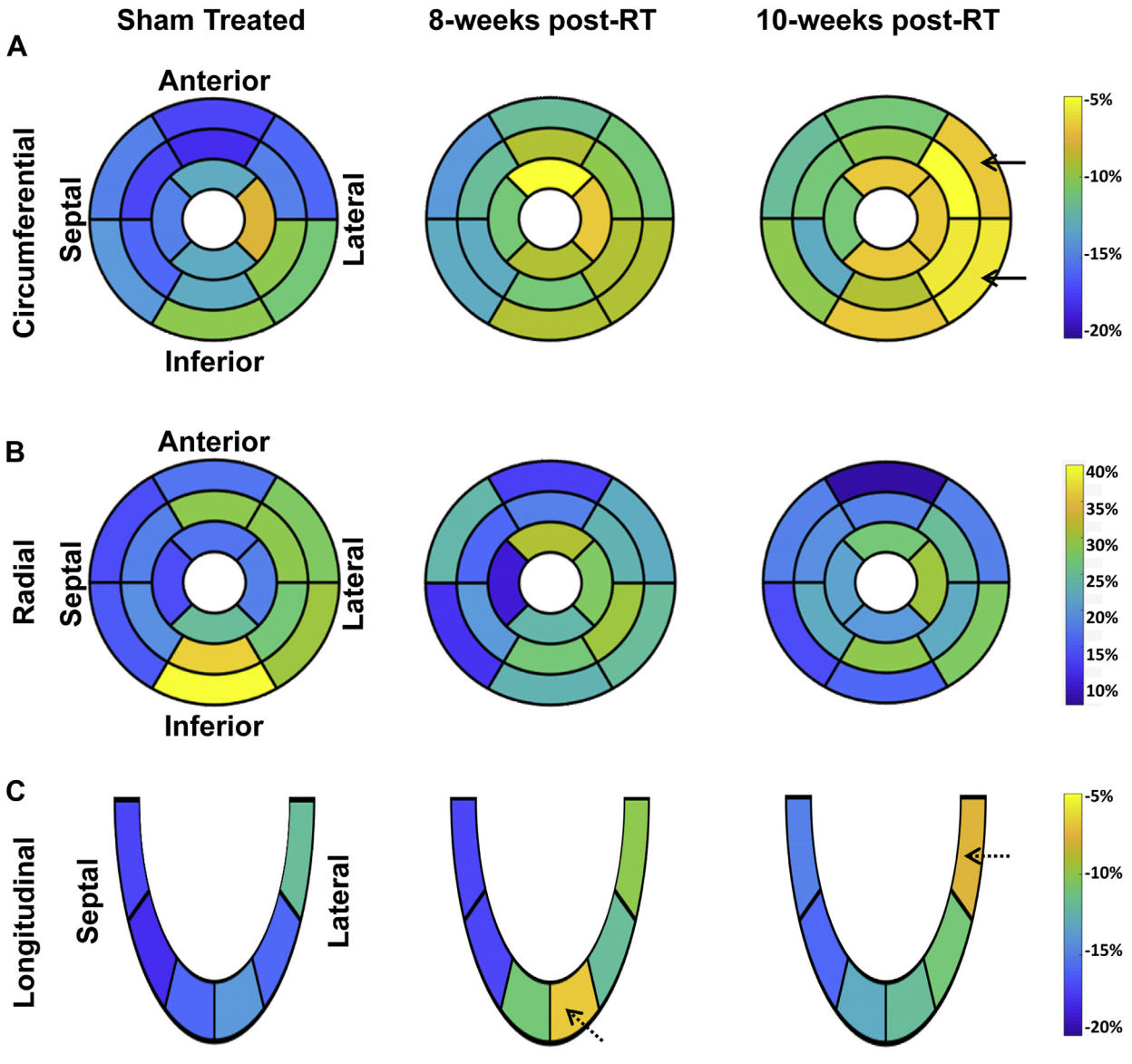

Segmental strain distribution in radiation therapy (RT) and sham-treated rats demonstrates reduced strain post-RT. Average segmental strain (**A**, circumferential; **B**, radial; **C**, longitudinal) in sham-treated, 8-week, and 10-week post-RT rats. The left-ventricular 17-segment model is used for presenting strain at the basal, mid-ventricular, and apical levels. **Blue and yellow** represent better and worse strain, respectively, in the circumferential and longitudinal directions, whereas the color interpretation is the opposite for radial strain (**blue and yellow** represent worse and better strain, respectively). Overall, strain values are reduced post-RT, which occurs differently in different myocardial segments and strain dimensions. Greater changes in strain are seen in the lateral wall **(solid arrows)** versus the septum for circumferential strain. Longitudinal strain showed apical and basal strain reduction at 8 weeks and 10 weeks post-RT, respectively **(dashed arrows)**.

responses to RT. Indeed, in this model of localized cardiac radiation in female SS rats, we have demonstrated increased mast cells (Figure 1) and T cells, including $CD8^+$ T cells, infiltrating the heart 10 weeks after radiation (16,25). This increase in inflammation may be responsible for the increased T2 values seen after cardiac radiation. In addition, the vacuolization and tissue changes seen on H&E staining may account

FIGURE 8 Segmental Tissue Displacement in RT and Sham-Treated Rats

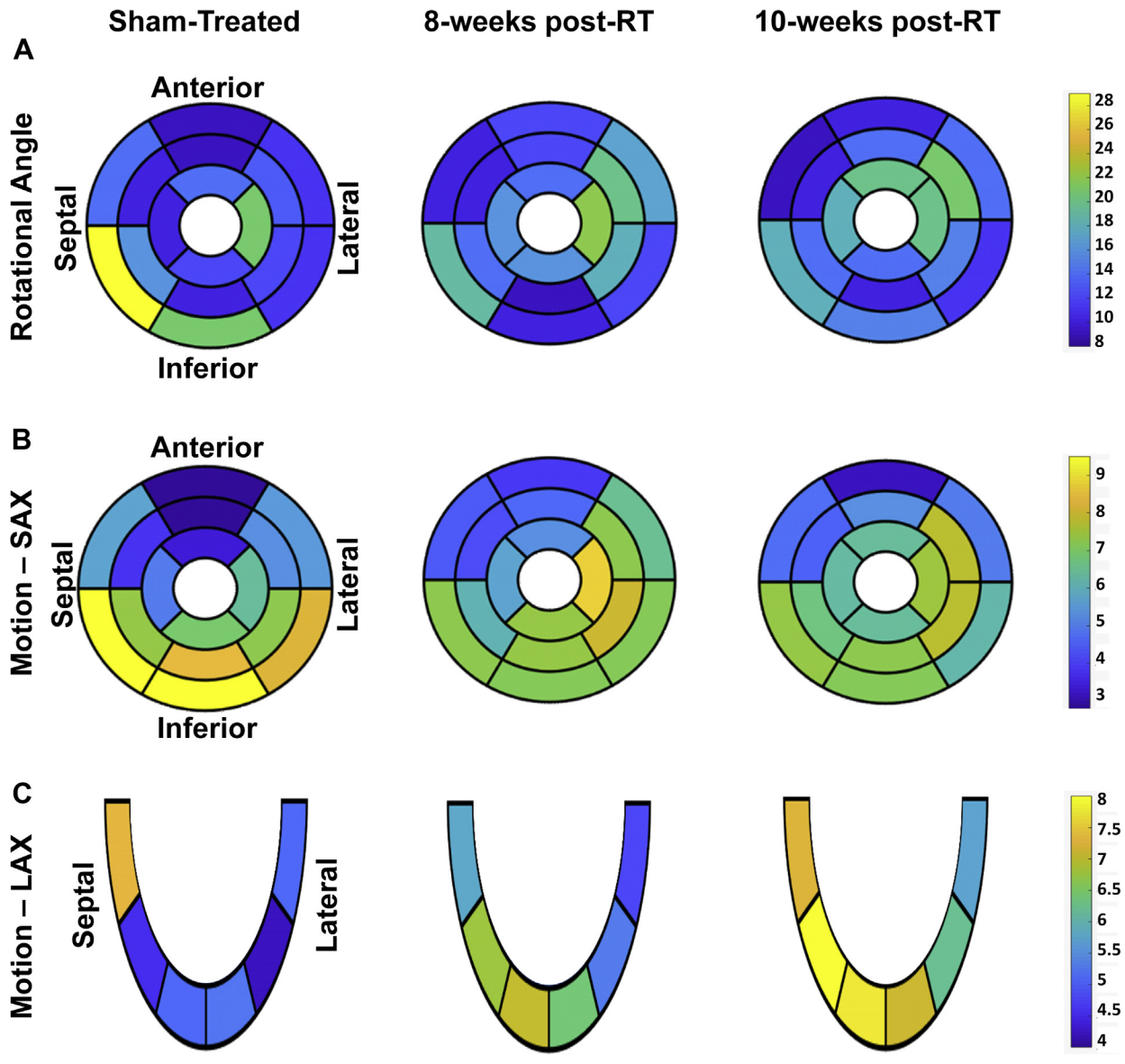

Segmental tissue displacement in RT and sham-treated rats demonstrate maintained tissue motion post-RT. Segmental distribution of average myocardial tissue displacement (**A**, rotation angle; **B**, SAX motion, mm; **C**, LAX motion, mm) in the left ventricle in sham-treated, 8-week, and 10-week post-RT rats. The left-ventricular 17-segment model is used for presenting values at basal, mid-ventricular, and apical levels. Note different tissue displacement values post-RT compared with the sham-treated rats, which differ based on location of the myocardial segment and type of displacement. Abbreviations as in Figure 4.

for T2 changes (29). The lack of significant changes in T1 values is consistent with the lack of significant increases in interstitial fibrosis at 10 weeks post-RT (Figure 3).

A number of rodent models, including ours, have shown overall preservation of function/EF initially after a high dose of cardiac RT (16,30), with eventual decreased EF by 5 to 6 months after RT. A key finding in this study is the importance of myocardial strain as early markers of RT-induced subclinical cardiac dysfunction despite preserved EF. The observed more significant abnormalities in circumferential and

TABLE 3 Myocardial Displacement Measurements in RT and Control (Sham-Treated) Rats

	8 Weeks			10 Weeks	
	Sham-Treated Control	Post-RT	p Value vs. Control	Post-RT	p Value vs. Control
Rotation angle, °					
Global	14.1 ± 1.0	14.4 ± 0.7	0.524	14.7 ± 0.7	0.393
Base	16.1 ± 1.3	13.3 ± 1.1	0.067	13.0 ± 0.6	0.029
Mid	11.9 ± 0.9	13.7 ± 1.0	0.108	14.1 ± 0.8	0.042
Apex	14.4 ± 1.5	17.0 ± 1.1	0.098	18.0 ± 1.5	0.057
SAX, mm					
Global	6.1 ± 0.4	6.3 ± 0.3	0.444	6.2 ± 0.3	0.559
Base	6.9 ± 0.4	6.0 ± 0.3	0.079	5.6 ± 0.2	0.015
Mid	5.9 ± 0.5	6.3 ± 0.4	0.343	6.6 ± 0.4	0.146
Apex	5.4 ± 0.4	6.8 ± 0.1	0.006	6.7 ± 0.5	0.026
LAX, mm					
Global	5.2 ± 0.3	6.0 ± 0.7	0.196	7.0 ± 0.5	0.005
Base	6.2 ± 0.6	5.3 ± 0.3	0.081	6.4 ± 0.4	0.493
Mid	4.4 ± 0.1	6.0 ± 0.4	0.008	7.1 ± 0.4	< 0.001
Apex	5.1 ± 0.1	6.7 ± 0.2	0.015	7.4 ± 0.1	< 0.001

Values are mean ± SEM. Myocardial rotation angle, short-axis motion (SAX), and long-axis motion (LAX) in nonirradiated control and radiation therapy (RT) rats at the base, mid-ventricular, and apical levels, and whole-heart global average (Global) value are shown.

longitudinal strain compared with radial strain may be attributed in part to cardiac remodeling and ventricular hypertrophy post-RT, which results in less changes in radial strain. Changes in radial strain may occur later after RT in this model, as previously shown (16).

This study demonstrates that myocardial segments with the greatest worsening in strain values were in the lateral region of the heart when compared with the septal region, even though there was not a notable difference in RT dose distribution between these areas. Histological examination of the LV also demonstrates increased vacuolization in the LV lateral wall versus the septal region (**Figures 2A to 2D**). Although it is possible that certain segments of the heart may be more sensitive to a given dose of RT, we cannot definitively conclude that from our findings, due to the lack of detailed segmental dosimetry data available for our studies. The use of small-animal CMR to assess subclinical changes after radiation can assist in elucidating the relative radiation sensitivity of different cardiac substructures. This will be especially helpful in determining regions where damage occurs after partial heart radiation, which is the clinical situation that occurs in most thoracic cancer patients who receive cardiac RT exposure.

STUDY LIMITATIONS. A limitation of the current study is the acquisition of T1 and T2 maps only at the mid-ventricular level to reduce scan time to ~1 h for animal welfare with anesthesia time. For the same reason, the CMR protocol used in this study did not include contrast-enhanced or flow imaging, which could have been used for assessing coronary artery, valvular, or pericardial diseases. However, the strain imaging included in this study provided valuable information about regional cardiac function that showed to correlate with regions of myocardial ischemia and infarction and is affected in different cardiomyopathies, valvular heart diseases, and pericardial diseases (14). It should be noted that RV strain analysis was not feasible in the current study due to thin RV wall with respect to tag spacing. Another limitation is that the sham rats were imaged at 8 weeks post-treatment, which should be taken in consideration when comparing results from the sham rats to those from the 10-week post-RT rats. It should be also noted that our model utilized rats that were not tumor-bearing, whereas patients exposed to cardiac radiation as part of their cancer treatment typically have intact tumors/tumor cells that are irradiated. However, in many situations, such as the majority of breast cancer patients treated with

FIGURE 9 T1 and T2 Maps of RT and Sham-Treated Rats

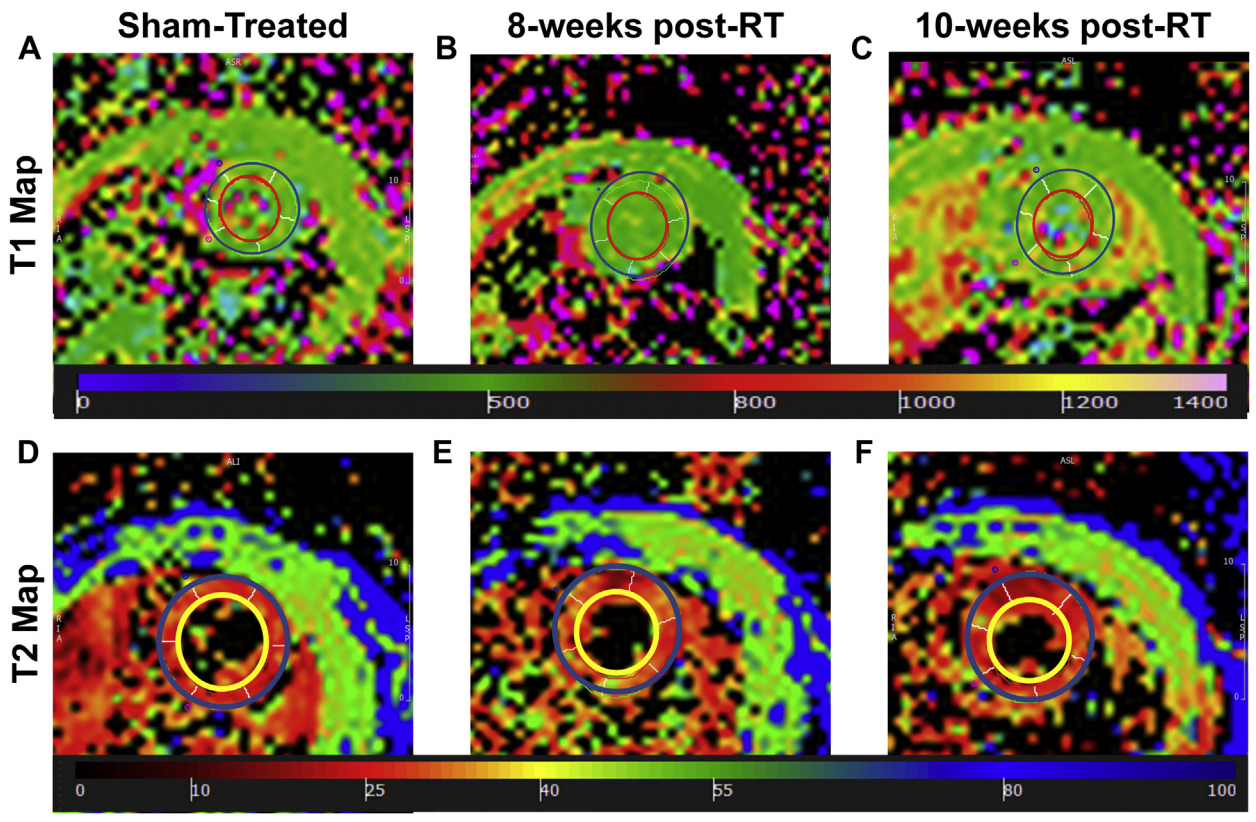

(A to C) Apparent T1 and **(D to F)** T2 maps of a mid-ventricular slice from **(A and D)** sham-treated, **(B and D)** 8-week post-radiation therapy (RT), and **(C and F)** 10-week post-RT rats (T1 and T2 measurements in milliseconds). Note the slight difference in values (color) between sham and RT rats.

RT, the cancer cells present may be microscopic and/or nondetectable. Finally, the addition of even earlier time points, when cardiac function may be preserved, but inflammatory changes may be occurring, may also be useful to shed insight into how T1 and T2 mapping may change after localized cardiac radiation.

CONCLUSIONS

Regional cardiac imaging by CMR provides detailed information about the functional patterns post-RT and allows for the early detection of RT-induced cardiotoxicity before worsening in EF is evident. Our histological studies support our CMR findings. Using these methods, quantitation of strain across different dimensions and segments allow for the detailed assessment of spatial and temporal progression of regional cardiac dysfunction post-RT. This knowledge is valuable for better understanding the segmental radiation effects on the heart, and with further study may allow for the early initiation of cardioprotective therapy with the potential to inform radiation treatment planning to reduce RT-induced cardiotoxicity.

FUNDING SUPPORT AND AUTHOR DISCLOSURES

The study was funded by the Daniel M. Soref Charitable Trust, Center for Imaging Research, Medical College of Wisconsin (Drs. Ibrahim and Bergom) and supported by NIH NHLBI grant 1R01HL147884 (Dr. Bergom). Additional support was provided by the Mary Kay Foundation Award Grant No. 017-29 (Dr. Bergom),

CENTRAL ILLUSTRATION **Strain Measurements in Radiation Therapy and Sham Rats**

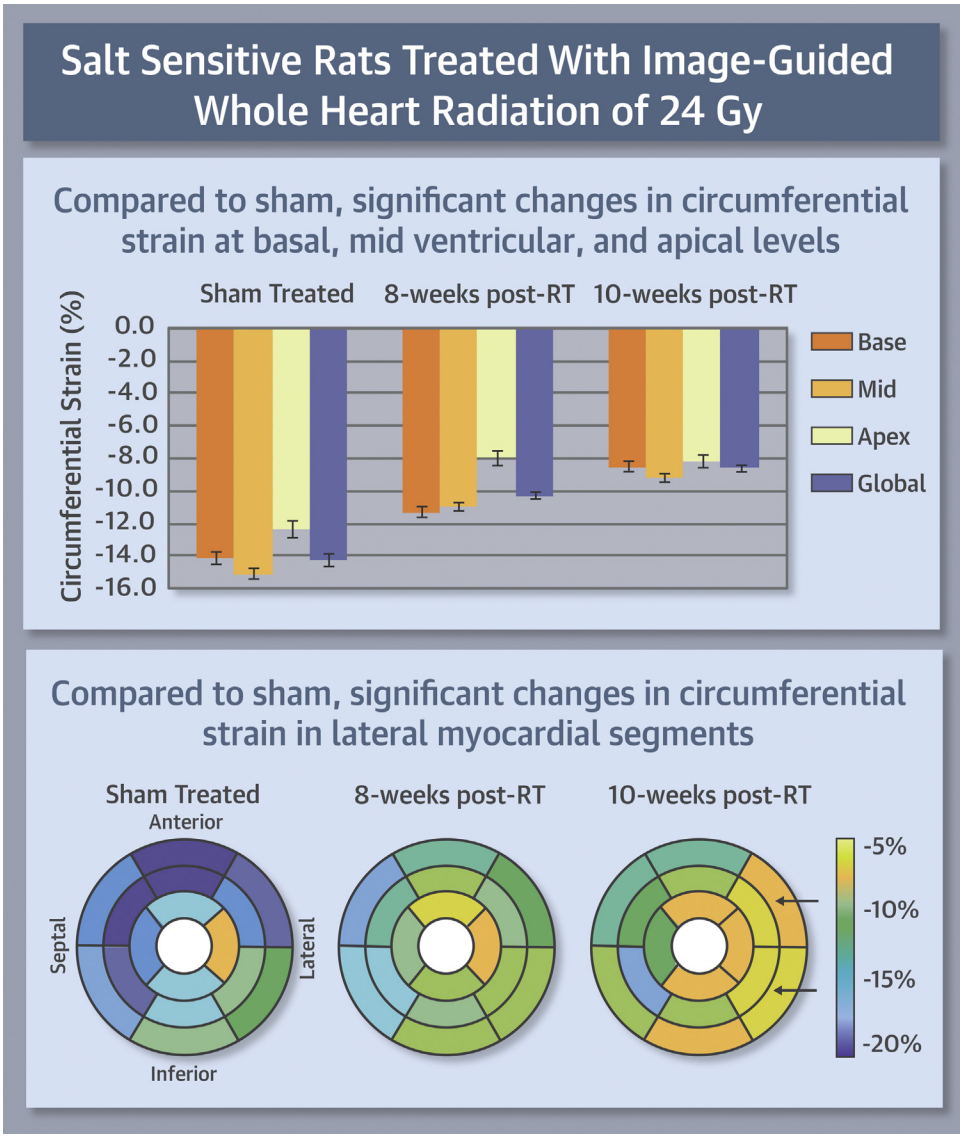

Ibrahim, E.-S.H. et al. J Am Coll Cardiol CardioOnc. 2021;3(1):113–30.

Strain measurements in radiation therapy (RT) and sham rats reveal early worsening in strain, especially in the circumferential direction, post-RT. Compared with sham treatment, circumferential strain changes occurred at the basal, mid-ventricular, and apical levels ($p < 0.05$ for all), especially at the lateral regions, which suggests that circumferential strain a sensitive marker of RT-induced cardiotoxicity.

Susan G. Komen® Grant CCR17483233 (Dr. Bergom), the Nancy Laning Sobczak, PhD, Breast Cancer Research Award (Dr. Bergom), the Medical College of Wisconsin Cancer Center (Dr. Bergom), the Michael H. Keelan, Jr., MD, Research Foundation Grant (Dr. Bergom), and the Cardiovascular Center at the Medical College of Wisconsin, (Dr. Bergom). Dr. Flister is currently employed at Abbvie, but not at the time of this work. Dr. Bergom has received research funding from Innovation Pathways. All other authors have reported that they have no relationships relevant to the contents of this paper to disclose.

ADDRESS FOR CORRESPONDENCE: Dr. El-Sayed Ibrahim, Department of Radiology, Medical College of Wisconsin, 8701 West Watertown Plank Road, Milwaukee, Wisconsin 53226, USA. E-mail: eibrahim@mcw.edu. Twitter: @sayed_phd, @carmenbergom, @dhiraj57302028, @PierreCroisille, @JStojanovskaMD, @jruben4, @LaviolettePeter.

PERSPECTIVES

COMPETENCY IN MEDICAL KNOWLEDGE: This study illustrates the capabilities of regional myocardial strain imaging by CMR imaging for the early detection of RT-induced subclinical cardiac dysfunction before global cardiac function, as assessed by ejection fraction, is affected. A worsening in strain was particularly notable at 10 weeks post-RT, with greatest changes in circumferential at the basal, mid-ventricular, and apical levels. Lateral myocardial segments showed significant changes in strain measurements at 10 weeks post-RT. Histological changes supported the changes seen on CMR imaging.

TRANSLATIONAL OUTLOOK: With additional study, regional myocardial strain by CMR may inform how we treat and monitor cancer patients treated with radiation, and allow for the early detection of patients at risk for cardiotoxicity. Furthermore, identification of cardiac substructures that are vulnerable to RT injury could allow for optimized treatment planning. With further investigation, these data could also be used to build models for predicting cardiotoxicity risk in patients.

REFERENCES

1. Darby SC, Ewertz M, McGale P, et al. Risk of ischemic heart disease in women after radiotherapy for breast cancer. N Engl J Med 2013;368:987–98.

2. Donnellan E, Phelan D, McCarthy CP, Collier P, Desai M, Griffin B. Radiation-induced heart disease: A practical guide to diagnosis and management. Cleve Clin J Med 2016;83:914–22.

3. Dess RT, Sun Y, Matuszak MM, et al. Cardiac events after radiation therapy: combined analysis of prospective multicenter trials for locally advanced non-small-cell lung cancer. J Clin Oncol 2017;35:1395–402.

4. Wang K, Pearlstein KA, Patchett ND, et al. Heart dosimetric analysis of three types of cardiac toxicity in patients treated on dose-escalation trials for Stage III non-small-cell lung cancer. Radiother Oncol 2017;125:293–300.

5. Speirs CK, DeWees TA, Rehman S, et al. Heart dose is an independent dosimetric predictor of overall survival in locally advanced non-small cell lung cancer. J Thorac Oncol 2017;12:293–301.

6. Haque W, Verma V, Fakhreddine M, Butler EB, Teh BS, Simone CB 2nd, Trends in cardiac mortality in patients with locally advanced non-small cell lung cancer. Int J Radiat Oncol Biol Phys 2018;100:470–7.

7. Bradley JD, Paulus R, Komaki R, et al. Standard-dose versus high-dose conformal radiotherapy with concurrent and consolidation carboplatin plus paclitaxel with or without cetuximab for patients with stage IIIA or IIIB non-small-cell lung cancer (RTOG 0617): a randomised, two-by-two factorial phase 3 study. Lancet Oncol 2015;16:187–99.

8. Zhang TW, Snir J, Boldt RG, et al. Is the importance of heart dose overstated in the treatment of non-small cell lung cancer? A systematic review of the literature. Int J Radiat Oncol Biol Phys 2019;104:582–9.

9. Schlaak RA, SenthilKumar G, Boerma M, Bergom C. Advances in preclinical research models of radiation-induced cardiac toxicity. Cancers (Basel) 2020;12:415.

10. Johnson CB, Sulpher J, Stadnick E. Evaluation, prevention and management of cancer therapy-induced cardiotoxicity: a contemporary approach for clinicians. Curr Opin Cardiol 2015;30:197–204.

11. Higgins AY, O'Halloran TD, Chang JD. Chemotherapy-induced cardiomyopathy. Heart Fail Rev 2015;20:721–30.

12. Kongbundansuk S, Hundley WG. Noninvasive imaging of cardiovascular injury related to the treatment of cancer. J Am Coll Cardiol Img 2014;7:824–38.

13. Choi EY, Rosen BD, Fernandes VR, et al. Prognostic value of myocardial circumferential strain for incident heart failure and cardiovascular events in asymptomatic individuals: the Multi-Ethnic Study of Atherosclerosis. Eur Heart J 2013;34:2354–61.

14. Ibrahim EH. Heart Mechanics: Magnetic Resonance Imaging. Boca Raton, FL: CRC Press, 2017.

15. Zagar TM, Cardinale DM, Marks LB. Breast cancer therapy-associated cardiovascular disease. Nat Rev Clin Oncol 2016;13:172–84.

16. Schlaak RA, Frei A, Schottstaedt AM, et al. Mapping genetic modifiers of radiation-induced cardiotoxicity to rat chromosome 3. Am J Physiol Heart Circ Physiol 2019;316:H1267–80.

17. Ibrahim EH, Baruah D, Budde M, Rubenstein J, Frei A, Schlaak RA, et al. Optimized cardiac functional MRI of small-animal models of cancer radiation therapy. Magn Reson Imaging 2020;73:130–7.

18. Ibrahim EH, Stojanovska J, Hassanein A, et al. Regional cardiac function analysis from tagged MRI images. Comparison of techniques: Harmonic-Phase (HARP) versus Sinusoidal-Modeling (SinMod) analysis. Magn Reson Imaging 2018;54:271–82.

19. Flister MJ, Hoffman MJ, Lemke A, et al. SH2B3 is a genetic determinant of cardiac inflammation and fibrosis. Circ Cardiovasc Genet 2015;8:294–304.

20. Rybin VO, Grabham PW, Elouardighi H, Steinberg SF. Caveolae-associated proteins in cardiomyocytes: caveolin-2 expression and interactions with caveolin-3. Am J Physiol Heart Circ Physiol 2003;285:H325–32.

21. Dedkov EI, Zheng W, Christensen LP, Weiss RM, Mahlberg-Gaudin F, Tomanek RJ. Preservation of coronary reserve by ivabradine-induced reduction in heart rate in infarcted rats is associated with decrease in perivascular collagen. Am J Physiol Heart Circ Physiol 2007;293:H590–8.

22. Di Marco GS, Reuter S, Kentrup D, et al. Cardioprotective effect of calcineurin inhibition in an animal model of renal disease. Eur Heart J 2011;32:1935–45.

23. Tirziu D, Chorianopoulos E, Moodie KL, et al. Myocardial hypertrophy in the absence of external stimuli is induced by angiogenesis in mice. J Clin Invest 2007;117:3188–97.

24. Zheng W, Brown MD, Brock TA, Bjercke RJ, Tomanek RJ. Bradycardia-induced coronary angiogenesis is dependent on vascular endothelial growth factor. Circ Res 1999;85:192–8.

25. Schlaak RA, Frei A, Fish BL, et al. Acquired immunity is not essential for radiation-induced heart dysfunction but exerts a complex impact on injury. Cancers (Basel) 2020;12:983.

26. Reshko LB, Kalman NS, Hugo GD, Weiss E. Cardiac radiation dose distribution, cardiac events and mortality in early-stage lung cancer treated with stereotactic body radiation therapy (SBRT). J Thorac Dis 2018;10:2346–56.

27. Pieters RS, Wagner H, Baker S, et al. The impact of protocol assignment for older adolescents with Hodgkin lymphoma. Front Oncol 2014; 4:317.

28. Kim PK, Hong YJ, Im DJ, et al. Myocardial T1 and T2 mapping: techniques and clinical applications. Korean J Radiol 2017; 18:113–31.

29. Galan-Arriola C, Lobo M, Vilchez-Tschischke JP, et al. Serial magnetic resonance imaging to identify early stages of anthracycline-induced cardiotoxicity. J Am Coll Cardiol 2019; 73:779–91.

30. Mezzaroma E, Di X, Graves P, et al. A mouse model of radiation-induced cardiomyopathy. Int J Cardiol 2012;156:231–3.

KEY WORDS cardiotoxicity, ejection fraction, heart, MRI, radiation therapy, rat, strain

APPENDIX For supplemental videos, please see the online version of this paper.